

Transactions on
Computational Modeling
and Intelligent Systems

Volume 4, July 2026, Article 10080
https://doi.org/10.65112/tcmis.10080

eISSN: 3108-5202
www.tcmis.org

RESEARCH ARTICLE

Comparative study on heat and mass transfer performance of ternary hybrid nanoliquid over an exponentially stretching surface

Gangadhar Poojari Ashwinkumar[1*], Uppar Shivakumar[1], Bhandare Ranjana[1,2], and Pradeep Nanda[1,3]

[1] *Department of Mathematics, Vijayanagara Sri Krishnadevaraya University, Ballari, Karnataka, India.*
[2] *Department of Mathematics, Government First Grade College, Haliyal 581329, India.*
[3] *Department of Mathematics, Government First Grade College, Yelburga 583236, India.*

[*] *Corresponding Author. Email: ashwinpuje@gmail.com (G.P. Ashwinkumar)*

Article Information

Received: 14 April 2026
Accepted: 22 July 2026
Published: 25 July 2026

AMS 2020 Classification:
76W05, 76D10, 76-10

Abstract

Nowadays, enhanced heat transfer in conventional liquids is a major task in several nanotechnological applications. This work addresses the above issue by exploring the intuition behind hybrid nanoliquids by augmenting the thermal conductivity of a conventional liquid. For this, we performed a comparative analysis to evaluate the superior heat conduction properties of the three diverse solutions, namely nanoliquid, hybrid nanoliquid and ternary hybrid nanoliquid flow above an exponentially stretched surface under the action of uneven heat rise/fall effects. For the estimation of the enhanced thermal conductivity, three distinct systems were analyzed: a water-based Al nanofluid (NF), an Al+AA7072 hybrid mixture (HNF), and a tri-hybrid composition (THNF) consisting of Al+AA7072+AA7075, and we discussed the results in detail using simultaneous outcomes. The transformed governing equations are solved numerically using the MATLAB bvp5c solver. The influences of magnetic field, thermal radiation, non-uniform heat source/sink, chemical reaction, and nanoparticle volume fraction on the velocity, temperature, concentration, local Nusselt number, and Sherwood number are systematically investigated. The results demonstrate that the ternary hybrid nanoliquid exhibits superior heat- and mass-transfer performance compared with the corresponding hybrid and mono nanofluids.

Keywords: Magnetohydrodynamics, heat transfer, exponential stretched surface, nanofluid, and thermal radiation

1. Introduction

A nanofluid refers to a colloidal mixture where sub-micron particles are dispersed within a carrier medium. Nanoliquids exhibit an elevated thermal capacity and greater stability when combined with base fluids. These liquids typically offer superior Heating and refrigerating performance in Numerous engineering applications, including built-up procedures, microchip cooling, and astrophysical cooling systems. The study of nanoliquids originated with Choi and Eastman [1]. Later, the role of solar energy on the Lorentz force-influenced motion of nanofluids in a planar domain was analyzed via numerical techniques by Ghasemi et al. [2] using Rosseland approximation across a stretching plate. Eid [3] simulated the power of Thermal energy production under an MHD stream of nanoliquid above an exponentially stretching sheet. Ahmad and others [4] employed the Maxwell model to study the thermal transport characteristics of a water ferrofluid past a bidirectionally expanding exponential sheet. Moreover, Sulochana et al. [5] examined the effect of the Buongiorno slip mechanism on magnetohydrodynamic nanofluid flows over a permeable stretched surface and concluded that the energy transmission rate is enhanced with increasing Soret number. The current advances in analysing the energy-transfer performance of nanoliquids are reported in [6-10].

Later, Ghadikolaei et al. [11] numerically examined the dynamics of an MHD Casson nanoliquid past a nonlinear permeable spreading sheet with radiation. Further, Srinivasacharya and others [12] scrutinized the implications of velocity slip and ohmic heating, together with convective edge effects, over a stretched sheet. The motion of Oldroyd-B nanoliquid throughout an exponentially stretched region in the presence of microbes was discussed by Muhammad et al. [13]. The significance of extended heat flux for an MHD motion across a time-dependent, expanding region was established by Ahmed et al. [14]. Later, Seid et al. [15] theoretically simulated the cause of porosity and the effect of an applied magnetic field on a nanofluid stream in a vertically stretched region. The flow and energy transport behaviour of Maxwell nanoliquid under the control of heat radiation and chemical responses along an extending surface was clarified by the authors [16, 17].

Additionally, the thermal efficiency of nanoliquids is significantly enhanced by combining two distinct nanoparticles with similar or varying volumes in the base fluid, forming mixed or hybrid nanofluids. Compared with mono-nanofluids, these mixed nanofluids act as more effective heat-transfer agents. Many researchers presented their work on these advanced fluid types. Masoud et al. [18] experimentally studied the implications of nanomaterials pertaining to the rheological nature of $Fe_3O_4 - Ag/EG$ mixed nanoliquid. The Investigation on the impact of an induced magnetic force on stagnation-point movement for a past-extending plan was reported by Iqbal et al. [19]. Meanwhile, Hayat et al. [20] utilised a 3D pattern to witness the consequences of thermal emission and molecular interactions. The characteristics of the spinning flow of a $Cu - Al_2O_3$ Mixed nanoliquid with nonlinear radiation were modelled by Usman and colleagues [21].

The comparative motion analysis of three-dimensional MHD nanofluid and hybrid nanofluid across a stretching plane of uneven thickness was given by the researchers [22]. Later, Urmi and others [23] experimentally scrutinized the thermo-physical characteristics of $TiO_2 - Al_2O_3$ mixed nanofluid containing 0% ethylene glycol-based solvent. Sreedevi et al. [24] addressed the energy and mass transport phenomena of an electromagnetically influenced hybrid nanoliquid past a spreading sheet with suction and chemical effects. Further, Madhukesh et al. [25] performed the motion of a mixed nanoliquid ahead of a nonlinear, expanding boundary subjected to convective-type heating.

Recently, several researchers have found that tri-hybrid nanofluids demonstrate enhanced thermal conductivity when measured against dual-component hybrid systems. Ternary mixed nanofluids are a mixture of metallic or non-metallic oxides of three different nanomaterials in the elementary fluid. Hazarika et al. [26] examined the stream containing three nanoparticles Cu, Ag and Fe_3O_4 across a porous stretched geometry. Puneet et al. [27] addressed the stream and thermal transport nature of trihybrid nanofluids utilizing a refined Buongiorno model in the presence of bio-active mixers. The Motion and energy transport features of a trihybrid nanofluid across a curved, enlarged domain, as elaborated by Buongiorno's concept, were elaborated by Sarada and co-workers [28]. Building on this, Manjunath et al. [29] explained the Momentum and heat patterns transfer mechanism of ternary nanoliquid over a linear extending surface. The velocity analysis of a ternary hybrid nanoliquid along a vertical thermal cylinder is interpreted by Nazir et al. [30]. The entropy analysis of nanoparticles with H_2O+EG base liquid was discussed by Sohail et al. [31]. Additionally, Farhan et al. [32] investigated the stasis-point flow behaviour of a trihybrid nanoliquid past a stretchy rotating disc. The relative flow analysis of a graphene/magnesium oxide mixed nanofluid and a graphene/zirconium oxide/magnesium oxide trihybrid nanofluid, along with the slip effect across a moving plate, was presented by Prakash et al. [33].

Although several studies have investigated heat transfer in mono, hybrid, and ternary hybrid nanofluids over stretching surfaces, most have focused on a single fluid configuration or considered limited physical mechanisms. A systematic comparison of the thermal performance of Water–Al, Water–Al+AA7072, and Water–Al+AA7072+AA7075 nanofluids under identical flow conditions, including magnetohydrodynamic effects, thermal radiation, non-uniform heat source/sink, and chemical reaction, has received comparatively little attention. The present work addresses this gap by providing a unified computational framework to evaluate the influence of these governing parameters on momentum, thermal, and concentration fields, thereby identifying the relative heat-transfer enhancement achieved by ternary hybrid nanofluids.

The novelty of the present work lies not in introducing a new numerical algorithm or a new stretching-sheet model, but in establishing a unified comparative framework for evaluating the thermal performance of mono, hybrid, and ternary hybrid nanofluids under identical physical conditions. This approach enables the direct quantification of the incremental heat-transfer enhancement achieved through successive incorporation of multiple nanoparticles, which has received limited attention in previous studies.

Motivated by the aforementioned investigations, this research seeks to evaluate the heat transmission efficiency across three distinct fluid categories, namely traditional nanofluids, dual-hybrid, and tri-hybrid flow above an exponentially stretched surface under the action of uneven heat rise/fall effects. The original Problem is transformed into a boundary restricted model of a first-order Ordinary Differential Equation using the similarity method, and then tackled invoking the bvp5c MATLAB tool. The nature of the properties on streamlines and isotherms for various physical constraints on Motion and heat dissipation performance is illustrated in simple

diagrams. For the purpose of simplification, simultaneous solutions are provided for ternary hybrid, hybrid and simple nano-liquids.

The remainder of this paper is organized as follows. Section 2 presents the mathematical formulation of the physical model together with the governing equations and associated boundary conditions. Section 3 describes the similarity transformations, numerical methodology, and the evaluation of engineering quantities of interest. Section 4 discusses the numerical results and the physical interpretation of the effects of various governing parameters on the flow, thermal, and concentration fields. Finally, Section 5 summarizes the major findings and concluding remarks of the present study.

2. Mathematical modelling

Figure 1 illustrates the physical configuration of the present problem. A two-dimensional, steady, incompressible, electrically conducting ternary hybrid nanofluid flows over an exponentially stretching sheet. with stretching velocity $u = u_w = U_0 e^{x/l}$ and wall temperature $T(x) = T_\infty + T_0 e^{x/2l}$.

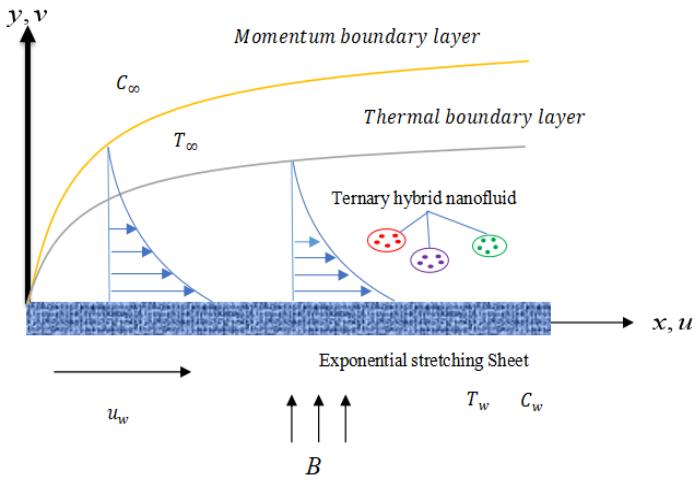


Figure 1. Flow configuration.

The x-axis is taken along the stretching surface, while the y-axis is normal to it. The sheet stretches with an exponential velocity, generating a boundary layer adjacent to the surface. A uniform transverse magnetic field is applied perpendicular to the flow direction. The surface is maintained at an exponentially varying temperature, whereas the ambient fluid is kept at a constant temperature. Thermal radiation, non-uniform heat source/sink, and chemical reaction effects are incorporated into the model. Under the boundary-layer approximations, the governing conservation equations are formulated and subsequently transformed into a system of ordinary differential equations using suitable similarity transformations.

The exponentially varying wall temperature is adopted to model practical manufacturing processes in which the heating intensity is intentionally varied along the stretching direction. Such thermal conditions arise in polymer extrusion, continuous metal strip processing, hot rolling, glass-fiber production, and coating technologies, where localized heaters, induction heating systems, or variable energy inputs generate non-uniform surface temperatures. Consequently, the exponential thermal boundary condition provides a physically meaningful representation of spatially varying heating encountered in industrial thermal processing and enables a realistic assessment of the resulting heat-transfer characteristics.

Considering the above-described conditions, the fundamental conservation equations for the fluid flow are formulated as stated below,

$$u_x + u_y = 0, \tag{1}$$

$$u(u_x) + v(u_y) = \frac{\mu_{tnf}}{\rho_{tnf}} u_{yy} - \frac{\sigma_{tnf}}{\rho_{tnf}} B_0^2 u, \tag{2}$$

$$uT_x + vT_y = \frac{k_{tnf}}{(\rho Cp)_{tnf}} T_{yy} + \frac{16\sigma^* T_\infty^3}{3k^* (\rho Cp)_{tnf}} T_{yy} + \frac{1}{(\rho Cp)_{tnf}} q''', \tag{3}$$

$$uC_x + vC_y = -Kr(C - C_\infty) + D_B C_{yy}, \tag{4}$$

with proper edge constraints

$$\left.\begin{array}{l} u = u_w = \dfrac{U_0}{e^{-x/l}}, v = 0,\ T = T_0,\ C = C_0 \quad \text{at } y = 0 \\ u \to 0,\ T \to T_\infty,\ C \to C_\infty \quad \text{as } y \to \infty \end{array}\right\}, \tag{5}$$

here [*u, v*] represent the flow velocity projections in the horizontal and vertical directions.

The material properties for the unary, hybrid, and tri-component nanofluid cases are defined as follows,

Property	**Nanofluid**
Viscosity	$\dfrac{\mu_{NF}}{\mu_F} = \left(1-\Phi_1\right)^{-2.5}$
Density	$\rho_{NF} = \rho_F\left(1-\Phi_1\right) + \rho_{P1}\Phi_1$
Specific heat capacity	$\left(\rho Cp\right)_{NF} = \left(\left(\rho Cp\right)_{P1} - \left(\rho Cp\right)_F\right)\Phi_1 + \left(\rho Cp\right)_F$
Thermal conductivity	$\dfrac{k_{NF}}{k_F} = \dfrac{2\left(k_F + k_{P1}\right) - k_{P1} - 2\Phi_1\left(k_F - k_{P1}\right)}{2\left(k_F + k_{P1}\right) - k_{P1} + \Phi_1\left(k_F - k_{P1}\right)}$
Electrical conductivity	$\dfrac{\sigma_{NF}}{\sigma_F} = \dfrac{\left(\sigma_{P1} + \sigma_F\right) + 2\Phi_1\left(\sigma_{P1} - \sigma_F\right)}{\left(\sigma_{P1} + \sigma_F\right) + \Phi_1\left(\sigma_F - \sigma_{P1}\right)}$

Property	**Hybrid nanofluid**
Viscosity	$\mu_{HNF} = \mu_F \dfrac{\left(1-\Phi_1\right)^{-2.5}}{\left(1-\Phi_2\right)^{2.5}}$
Density	$\dfrac{\rho_{HNF}}{\rho_F} = \left(1-\Phi_2\right)\left[\left(1-\Phi_1\right) + \Phi_1\dfrac{\rho_{P1}}{\rho_F}\right] + \Phi_2\left\{\dfrac{\rho_{P2}}{\rho_F}\right\}$
Specific heat capacity	$\dfrac{\left(\rho Cp\right)_{HNF}}{\left(\rho Cp\right)_F} = \left(1-\Phi_2\right)\left[\left(1-\Phi_1\right) + \Phi_1\dfrac{\left(\rho Cp\right)_{P1}}{\left(\rho Cp\right)_F}\right] + \Phi_2\dfrac{\left(\rho Cp\right)_{P2}}{\left(\rho Cp\right)_F}$
Thermal conductivity	$\dfrac{k_{HNF}}{k_{NF}} = \dfrac{k_{P2}\left(1+2\Phi_2\right) + 2k_{NF}\left(1+\Phi_2\right)}{k_{P2}\left(1-\Phi_2\right) + k_{NF}\left(2+\Phi_2\right)}$
Electrical conductivity	$\dfrac{\sigma_{HNF}}{\sigma_{NF}} = \dfrac{\left(\sigma_{P2} + \sigma_{NF}\right) + 2\Phi_2\left(\sigma_{P2} - \sigma_{NF}\right)}{\left(\sigma_{P2} + \sigma_{NF}\right) + \Phi_2\left(\sigma_{NF} - \sigma_{P2}\right)}$

Property	**Ternary hybrid nanofluid**
Viscosity	$\mu_{THNF} = \mu_F \dfrac{\left(1-\Phi_2\right)^{-2.5}}{\left(1-\Phi_1\right)^{2.5}\left(1-\Phi_3\right)^{2.5}} = A_1$
Density	$\dfrac{\rho_{THNF}}{\rho_F} = \left(1-\Phi_3\right)\left\{\left(1-\Phi_2\right)\left[\left(1-\Phi_1\right) + \Phi_1\dfrac{\rho_{P1}}{\rho_F}\right] + \Phi_2\dfrac{\rho_{P2}}{\rho_F}\right\} + \Phi_3\dfrac{\rho_{P3}}{\rho_F} = A_2$
Specific heat capacity	$\dfrac{\left(\rho Cp\right)_{THNF}}{\left(\rho Cp\right)_F} = \left(1-\Phi_3\right)\left\{\begin{array}{l}\left(1-\Phi_2\right)\left[\left(1-\Phi_1\right) + \Phi_1\dfrac{\left(\rho Cp\right)_{P1}}{\left(\rho Cp\right)_F}\right] \\ +\Phi_2\dfrac{\left(\rho Cp\right)_{P2}}{\left(\rho Cp\right)_F}\end{array}\right\} + \Phi_3\dfrac{\left(\rho Cp\right)_{P3}}{\left(\rho Cp\right)_F} = A_3$
Thermal conductivity	$\dfrac{k_{THNF}}{k_{HNF}} = \dfrac{k_{P3} + 2k_{HNF} - 2\Phi_3\left(k_{HNF} - k_{P3}\right)}{k_{P3} + 2k_{HNF} + \Phi_3\left(k_{HNF} - k_{P3}\right)}$
Electrical conductivity	$\dfrac{\sigma_{THNF}}{\sigma_{HNF}} = \dfrac{\left(\sigma_{P3} + \sigma_{HNF}\right) + 2\Phi_3\left(\sigma_{P3} - \sigma_{HNF}\right)}{\left(\sigma_{P3} + \sigma_{HNF}\right) - \Phi_3\left(\sigma_{P3} - \sigma_{HNF}\right)}$

The flow governing equations are altered by applying the following similarity aspects:

$$\left.\begin{aligned}
&\xi = e^{x/l},\ \eta = \sqrt{\frac{u_w}{2l\upsilon_f}}y, u = U_0 e^{x/l} F_\eta(\xi,\eta), u_w(x) = U_0 e^{x/l} \\
&v = -\sqrt{\frac{\upsilon_f U_0}{2l}} e^{\frac{x}{2l}} F(\xi,\eta) - \sqrt{\frac{2\upsilon_f U_0 \xi}{l}} \xi F_\xi(\xi,\eta) - y\frac{U_0}{2l}\xi F_\eta(\xi,\eta) \\
&\Theta = (T - T_\infty)(T_0 - T_\infty)^{-1},\ T(x) = T_\infty + T_0 e^{x/2l} \\
&\Psi = (C - C_\infty)(C_0 - C_\infty)^{-1},\ C(x) = C_\infty + C_0 e^{x/2l}
\end{aligned}\right\}, \tag{6}$$

Using Eq. (6), the nonlinear PDEs (2)-(4) are changed to the nonlinear ODEs as,

$$2(F_\eta^{\,2}) + 2\xi F_\eta(F_{\xi\eta}^2) = 2\xi(F_\xi)(F_{\eta\eta}) + \frac{1}{A_1 A_2}(F_{\eta\eta\eta}) - \frac{2}{A_2}\frac{\sigma_{tnf}}{\sigma_f}\frac{M}{\xi}F_\eta + F(F_{\eta\eta}), \tag{7}$$

$$\left.\begin{aligned}
A_3 \Pr\left[2\xi(F_\eta)(\Theta_\xi) + \Theta(F_\eta) - F(\Theta_\eta) - 2\xi(F_\xi)(\Theta_\eta)\right] = \left(\frac{k_{tnf}}{k} + Rd\right)(\Theta_{\eta\eta}) + \\
2\frac{k_{tnf}}{k_f} A_1 A_2 (F_\eta)(A^* F' + B^* \Theta)
\end{aligned}\right\}, \tag{8}$$

$$\xi F_\eta \Psi_\xi - \left(\frac{F}{2} + \xi F_\xi\right)\Psi_\eta = -k_0 \Psi + \frac{Sc}{2}(\Psi_{\eta\eta}), \tag{9}$$

The modified edge boundaries are,

$$\left.\begin{aligned}
&\frac{dF}{d\eta} = 1,\ F = -\xi\left(\frac{dF}{d\xi}\right),\ \Theta = 1, \Psi = 1, \text{ as } \eta = 0 \\
&\frac{dF}{d\eta} = 0,\ \Theta = 0, \Psi = 0 \quad as\ \ \eta \to \infty
\end{aligned}\right\}, \tag{10}$$

In the above Eqs. (7) – (9), the dimensionless constants $M, Pr, R\,d, Sc$ and q''' represent a magnetic field, Prandtl number, thermal radiation, Schmid number, and non-uniform heat source parameter, respectively. And given by the equation below,

$$\left.\begin{aligned}
&M = \frac{\sigma_F B_0^2 l}{U_0 \rho_F},\ \Pr = \frac{(\mu C_p)_F}{k_F},\ Rd = \frac{16\sigma^* T_\infty^3}{3k^* k_F},\ \text{Sc} = \frac{D_B}{\upsilon}, \\
&q''' = \frac{k_{tnf}}{x\upsilon_{tnf}} u[A^*(T_w - T_\infty) f' + B^*(T - T_\infty)]
\end{aligned}\right\}, \tag{11}$$

3. Methodological framework

To obtain a similarity solution, we consider the local boundary-layer approximation corresponding to the region where ξ <<1. Under this condition, the streamwise variations are much smaller than the transverse variations, and hence the derivative terms with respect to ξ become asymptotically negligible compared with the derivatives in the similarity variable. Consequently, the governing partial differential equations reduce to a system of ordinary differential equations representing the leading-order boundary-layer flow. Physically, this approximation is valid in the vicinity of the leading edge of the exponentially stretching surface, where the streamwise development of the boundary layer is relatively weak. Therefore, the present similarity solution should be interpreted as a local solution applicable within the range ξ <<1, rather than a global solution over the entire stretching surface.

In a comparable result, we take the derivative-bearing terms w.r.t. $\xi\,(i.e.(.)_\xi)$ in Eqs. (7) – (9) become minimal for ξ <<1 and prime denotes the ordinary derivative $\frac{d}{d\eta}$, Thus the Eqs. (7) – (9) become

$$\frac{1}{A_1 A_2} F''' - 2F'^2 + FF'' - \frac{2}{A_2}\frac{\sigma_{inf}}{\sigma_f}\frac{M}{\xi}F' - = 0, \tag{12}$$

$$\left(\frac{k_{tnf}}{k_f}+Rd\right)\Theta''+2\frac{k_{tnf}}{k_f}A_1A_2F'\left(A^*F'+B^*\Theta\right)-A_3\,\mathrm{Pr}\left(\Theta F'-F\Theta'\right)=0, \tag{13}$$

$$\frac{Sc}{2}\Psi''-k_0\Psi+\frac{F}{2}\Psi'=0, \tag{14}$$

with transformed edge conditions,

$$\left.\begin{aligned}&\frac{dF}{d\eta}=1,F=0,\Theta=1,\Psi=1,\ as\ \eta=0\\&\frac{dF}{d\eta}=0,\Theta=0,\Psi=0\ as\ \ \eta\to\infty\end{aligned}\right\}, \tag{15}$$

The dimensionless parameters of practical interest, specifically the surface drag coefficient, along with the rates of heat and mass transport, are formulated as:

$$\left.\begin{aligned}C_{fx}=\frac{\tau_w}{\rho_f U_w^2},\ \ Nu_x=\frac{2lq_w}{\left(T_w-T_\infty\right)k_f},\ \ Sh_x=\frac{xq_m\left(C_w-C_\infty\right)^{-1}}{D_B}\end{aligned}\right\}, \tag{16}$$

Wherein

$$\left.\begin{aligned}\tau_w=\mu_{tnf}\left(\frac{\partial u}{\partial y}\right)\Big|_{y=0},q_w=-\left(k_{tnf}+\frac{16\sigma^*T_\infty^3}{3k^*}\right)\left(T_y\right)\Big|_{y=0},q_m=-D_B\left(C_y\right)\Big|_{y=0}\end{aligned}\right\}, \tag{17}$$

Finally, we get

$$\left.\begin{aligned}&C_{fx}\,\mathrm{Re}_x^{1/2}=\frac{1}{A_1}f''(0),\\&Nu_x=-\mathrm{Re}_x^{1/2}\left(\frac{k_{tnf}}{k_f}+Rd\right)\theta'(0),\\&Sh_x=-\mathrm{Re}_x^{1/2}\frac{x}{2l}\phi'(0)\end{aligned}\right\}, \tag{18}$$

where $Re_x=\frac{2lU_w}{\upsilon_f}$ is the Reynolds number.

4. Numerical outcomes and discussion

In this segment, Eqs. (12) – (14), along with the edge restrictions (15). Numerically integrated utilizing the MATLAB bvp5c solver. The MATLAB package 'bvp5c' package is employed to achieve a numerical solution of the above equations. In this case, the higher-order differential equations are first converted into a system of first-order differential equations, and then the solutions are obtained. The step size represents the convergence criteria of the current study, $\Delta\eta=0.0001$, accurate to 5 decimal values. The inducement of non-dimensional constraints, viz., magnetic field (M), thermal radiative component (R), variable heat source (A^*, B^*), chemical response (kr), and Nanoparticle volume concentration (Φ) on rates of momentum, thermal, and mass flow is deliberated via plots. Further, these variables influence the surface drag coefficient, thermal, and mass transmission rate are depicted in tables for the Water + Al, Water + Al + AA7072, and Water + Al + AA7072 + AA7075 fluids. An analysis of the local Nusselt number for several physical factors is presented using a bar graph.

Figures 2–3 portray the significance of Mon momentum, energy and diffusion profiles for three diverse fluids under study. Evidently, temperature and mass curves are accelerating functions of M whereas velocity is a diminishing function. Physically, the added values of M develops a repulsive force, identified as Lorentz energy, in fluid flow. Owing to this, fluid velocity declines and temperature augments. The bearing of radiative heat flux on the thermal profiles is illustrated in Figure 4. We see that the swelling values of Rsupplies supplementation thermal energy to the fluid, making a thermal rise. It is very interesting to see that temperature distribution is more boosted in a ternary hybrid nanofluid.

Figures 5 and 6 reveal the responses of $A^*$and B^*on the temperature gradient. It is evident from the plots that the magnitudes of the temperature curves are elevated for the enhancement of both $A^*$and B^*. Generally, the upshot of $A^*$and B^*performances as energy originators due to this intensification in heat energy is noted. Figure 7 interprets the resteaverberation of Kr on the concentration gradient for three diverse working fluids. The rising

values of Kr causes a diminution in the molecular dispersion, which in turn reduces the concentration field. The implication of cumulative values of Φ on stream, thermal and concentration gradients are displayed in the Figures 8–10 respectively. Clearly, thermal and concentration gradients are amplified, but the velocity gradient decays. Physically, A higher concentration of nanoparticles elevates the fluid's internal friction, gives rise to reduced velocity and a concurrent expansion of the thermal and species concentration profiles. Figures 11–15 depict the Deviation in the Nusselt number for diverse range of M, R, A^*, B^* and Φ respectively.

The thermophysical characteristics of nanomaterials *Al*, *AA7072*, *AA7075*, and conventional liquid water are described in Table 1. Further, Tables 2, 3, and 4 portray the variation in the wall drag coefficient, rates of thermal and solute migration, respectively. It is observed that, C_{fx}, Nu_x and Sh_x diminishes with growing M. No change is recorded in the C_{fx} and Sh_x for enhancement in thermal radiation and uneven heat source parameters. Rate of energy transport in enhancing the volume fraction of the nanomaterial. More heat is transferred by ternary (*Water-Aluminium+AA7072+AA7075)* hybrid nanofluid in Correlation with the hybrid (*Water-Aluminium+AA7072*) nanofluid and mono (*Water-Aluminium*) nanofluid. The Species interaction constraint intensifies the rate of mass exchange. Furthermore, the mass transmission rate is much higher for the *Water-Aluminium+AA7072+AA7075* Tri-hybridized nanoliquid. Table 5 depicts the validation of the obtained results with the available literature for the limiting case and a good agreement between the results is witnessed.

Table 1. Thermal features of nano-additives and conventional liquid.

Property	***Water***	***Al***	***AA7072***	***AA7075***
$\rho\left(Kg/m^3\right)$	997.05	2712	2720	2810
$C_p\left(JKg^{-1}K^{-1}\right)$	4181.4	903	893	960
$k\left(Wm^{-1}K^{-1}\right)$	0.606	247	222	173
$\sigma\left(S/m\right)$	5.5X10^{-6}	3.5 X 10^{7}	34.83 X 10^{6}	26.77 X 10^{6}

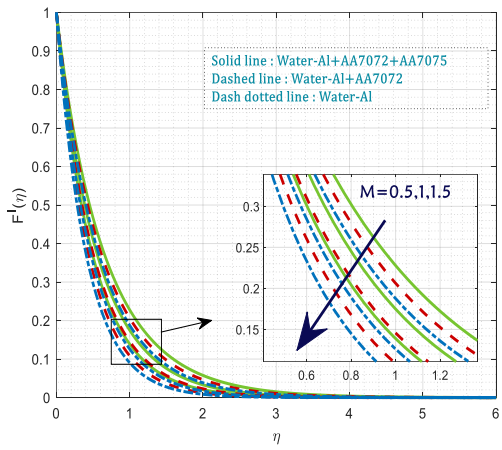


Figure 2. Result of M against $F^{|}(\eta)$.

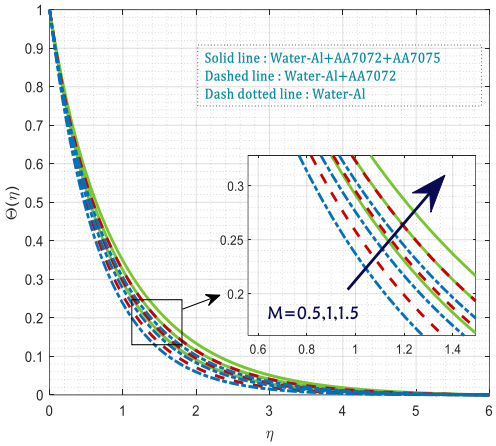


Figure 3. Result of M against $\Theta(\eta)$.

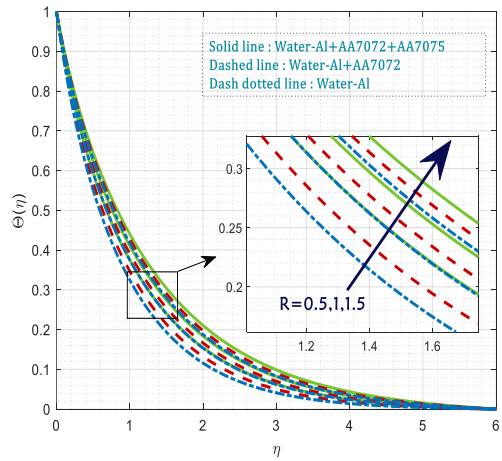


Figure 4. Result of R against $\Theta(\eta)$.

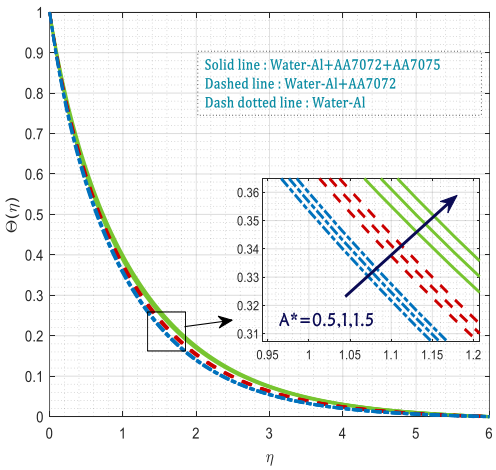


Figure 5. Result of A^* against $\Theta(\eta)$.

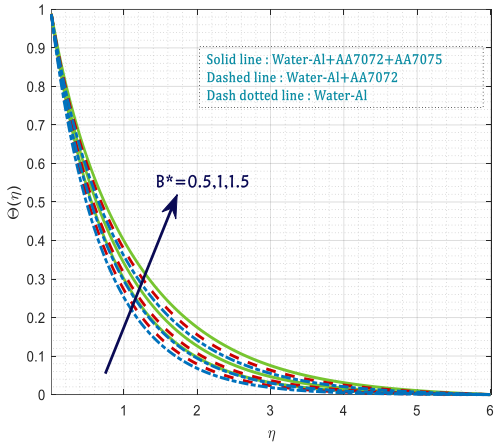


Figure 6. Result of B^* against $\Theta(\eta)$.

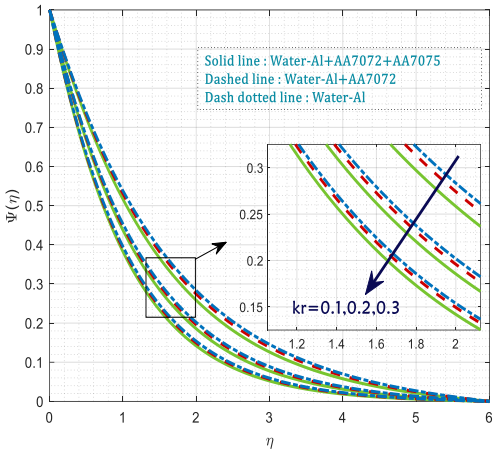


Figure 7. Effects of kr against $\Psi(\eta)$.

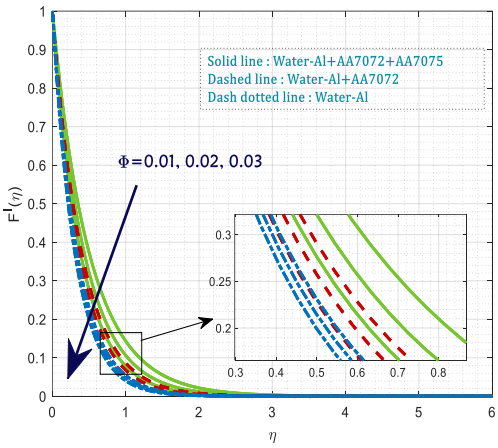


Figure 8. Effects of Φ against $F^{|}(\eta)$.

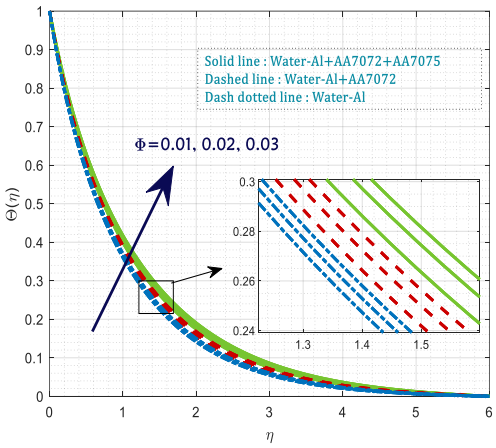


Figure 9. Outcome of Φ against $\theta(\eta)$.

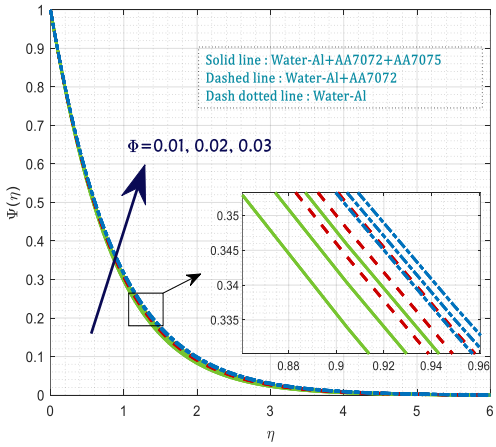


Figure 10. Outcome of Φ against $\Psi(\eta)$.

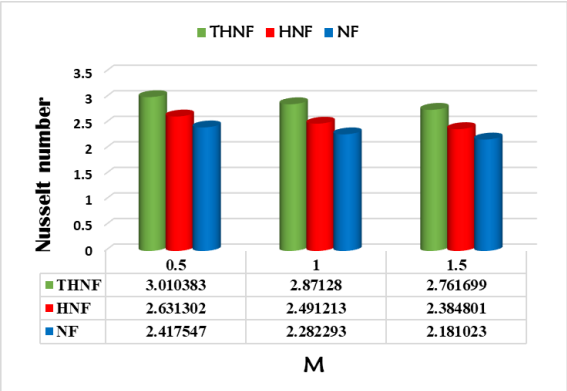


Figure 11. Variation in Nusselt number against M.

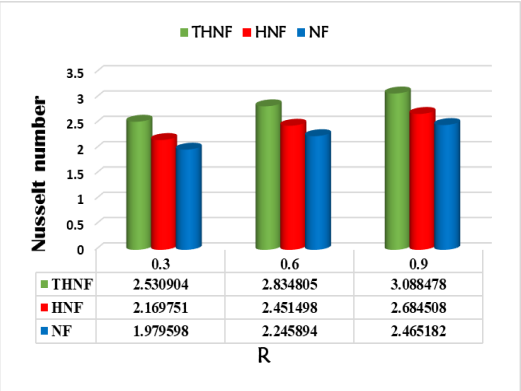


Figure 12. Nusselt number for distinct R.

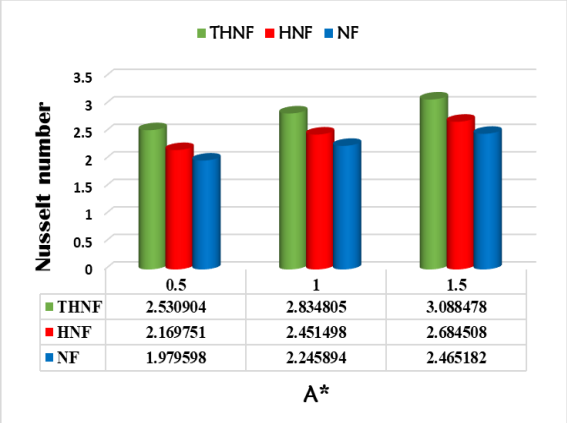


Figure 13. Nusselt Number against A^*.

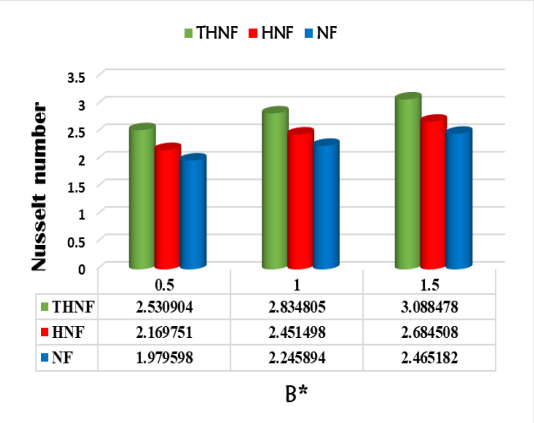


Figure 14. Nusselt Number for various B^*.

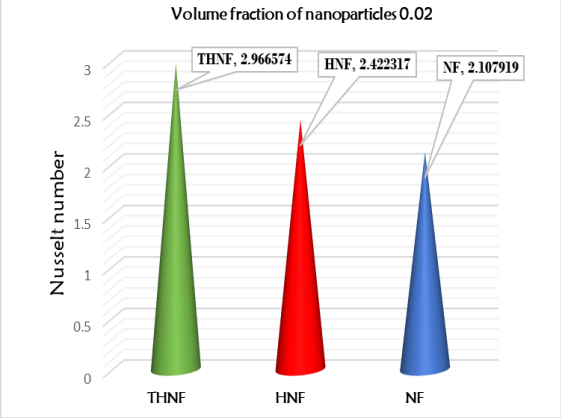


Figure 15. Heat transfer rate for $\Phi = 0.02$.

Table 2. Variation in wall friction component for ternary, hybrid and mono nanofluids.

M	Φ	Skin friction coefficient		
		Ternary nanofluid	Hybrid nanofluid	Nanofluid
0.5		-2.748644	-2.177712	-1.921859
1.0		-3.188708	-2.613745	-2.338142
1.5		-3.574249	-2.986274	-2.690366
	0.01	-4.537305	-3.895032	-3.542327
	0.02	-5.280849	-4.354013	-3.790477
	0.03	-6.165031	-4.868699	-4.054970

Table 3. Fluctuation in the local heat transport rate ternary, hybrid, and mono nanofluids.

M	R	A^*	B^*	Φ	Local Nusselt Number		
					Ternary nanofluid	Hybrid nanofluid	Nanofluid
0.5					3.010383	2.631302	2.417547
1.0					2.871280	2.491213	2.282293
1.5					2.761699	2.384801	2.181023
	0.3				2.457365	2.090379	1.895361
	0.6				2.565951	2.207112	2.018859
	0.9				2.665305	2.311656	2.127629
		0.5			2.530904	2.169751	1.979598
		1.0			2.681004	2.263682	2.052839
		1.5			2.831104	2.357614	2.126080
			0.5		2.530904	2.169751	1.979598
			1.0		2.834805	2.451498	2.245894
			1.5		3.088478	2.684508	2.465182
				0.01	2.530904	2.169751	1.979598
				0.02	2.735383	2.290178	2.041947
				0.03	2.966574	2.422317	2.107919

Table 4. Variation of Sherwood number for ternary, hybrid and mono nanofluids.

M	kr	Φ	Sherwood Number		
			Ternary nanofluid	Hybrid nanofluid	Nanofluid
0.5			1.150087	1.146000	1.142138
1.0			1.139427	1.132950	1.128119
1.5			1.131255	1.123506	1.118240
	0.1		0.613342	0.595992	0.585892
	0.2		0.774662	0.760972	0.752879
	0.3		0.904176	0.892554	0.885607
		0.01	1.114474	1.105241	1.099636
		0.02	1.117368	1.106793	1.100336
		0.03	1.121193	1.108836	1.101215

Table 5. Validation of obtained results for local Nusselt number.

Pr	Prakash et al. [33]	Present Results
0.2	0.17026	0.170262752
0.7	0.45445	0.454451586
2	0.91136	0.911368965
7	1.89540	1.895408935

5. Conclusion

An analytical assessment is undertaken to inspect the heat transport properties of nanofluid flow above exponential expansion of the boundary surface. The contribution of thermal radiation, molecular reaction, and nanoparticle volume fraction is also expounded.

The graphical results clearly demonstrate that the applied magnetic field suppresses the fluid velocity while enhancing the temperature and concentration distributions due to the Lorentz force. Thermal radiation and non-uniform heat generation significantly increase the thermal boundary-layer thickness, resulting in higher temperature profiles. An increase in the nanoparticle volume fraction improves the fluid's thermal performance but increases flow resistance due to the higher effective viscosity. Furthermore, the ternary hybrid nanofluid consistently exhibits superior heat-transfer performance compared with the hybrid and mono nanofluids, as evidenced by the temperature distributions and local Nusselt number plots. These observations confirm the effectiveness of ternary hybrid nanofluids in enhancing thermal transport in exponentially stretching surface applications.

Comprehensive results are contrasted for NF, HNF and THNF cases, yielding the following significant deductions.

- Improvements in the Lorentz force and nanomaterial density tend to reduce the wall shear stress, whereas no significant change is observed for additional thermal energy.
- An escalation in thermal radiation enhances the energy transfer rate, and this result is more significant in ternary mixed nanofluids as compared with mono and hybrid nanofluids.
- Also, the temperature is enhanced for augmenting values of uneven heat source and nanoparticle volume fraction factors.
- For lower frictional resistance of the flow, ternary hybrid nanofluid shows significant outcomes compared to the other two cases.
- The momentum and energy distributions are controllable via the Lorentz force and radiative heat transport.
- Considering three diverse solid nano-additives within the host medium is helpful for the augmented Energy transmission property of nanoliquids.

The author expresses his affectionate thanks to KSTePS DST, Government of Karnataka, India for the financial support under the grant (No. DST/KSTePS/Ph.D.Fellowship/MP-05/2024-25 dated 11th February 2025).

Acknowledgments

The authors state that no funding is involved.

Funding

The authors have no competing interests to declare that are relevant to the content of this article.

Conflict of interest

All authors contributed equally and approved the final manuscript.

Declaration of using AI tools

The authors declare that they have not used any type of generative artificial intelligence for the writing of this manuscript, nor for the creation of images, graphics, tables, or their corresponding captions.

References

[1] S. U. S. Choi and J. A. Eastman, “Enhancing thermal conductivity of fluids with nanoparticles,” ASME-Publications-Fed, vol. 66, pp. 99–105, 1995. 10.1115/IMECE1995-0926

[2] S. E. Ghasemi, M. Hatami, D. Jing, and D. D. Ganji, “Nanoparticles effects on MHD fluid flow over a stretching sheet with solar radiation: A numerical study,” J. Mol. Liq., vol. 219, pp. 890–896, 2016.

[3] M. R. Eid, “Chemical reaction effect on MHD boundary-layer flow of two-phase nanofluid model over an exponentially stretching sheet with a heat generation,” J. Mol. Liq., vol. 220, pp. 718–725, 2016.

[4] R. Ahmad, M. Mustafa, T. Hayat, and A. Alsaedi, “Numerical study of MHD nanofluid flow and heat transfer past a bidirectional exponentially stretching sheet,” J. Magn. Magn. Mater., vol. 407, pp. 69–74, 2016.

[5] C. Sulochana and G. P. Ashwinkumar, “Impact of Brownian moment and thermophoresis on the magnetohydrodynamic flow of magnetic nanofluid past an elongated sheet in the presence of thermal diffusion,” Multidiscip. Model. Mater. Struct., vol. 14, no. 4, pp. 744–755, 2018.

[6] Ashwinkumar, G. P., Ranjana, B., Sandeep, N., & Sulochana, C. Transpiration effect on magneto-flow of ternary hybrid nanofluid above an exponentially elongating sheet. Num. Heat Tran., Part B: Fundamentals, 2024; 1-18.

[7] Sandeep, N., P. Nanda, C. Sulochana, and G. P. Ashwinkumar. "Dynamics of Casson/Carreau hybrid nanofluid flow over a wedge with thermophoresis and Brownian motion effects." International Journal of Modelling and Simulation 2024; 1-12.

[8] Sandeep, N., U. Shivakumara, C. Sulochana, and G. P. Ashwinkumar. "Enhanced thermal conductivity of the Carreau nanoliquid by using Maxwell/Xue nanomodels." Num. Heat Tran., Part A: Applications (2024): 1-18.

[9] Sandeep, N., B. Ranjana, C. Sulochana, and G. P. Ashwinkumar. "Flow and heat transfer mechanism of engine-oil based hybrid nanofluid due to a nonlinearly extending surface: A comparative study." International Journal of Modelling and Simulation, 2023; 1-17.

[10] N. Sandeep, R. Suresh Babu, P. Nanda, and G. P. Ashwinkumar, "Enhanced heat transmission in conical slip flow of Walter'sB nanofluid," Int. J. Mod. Phys. B, vol. 38, no. 07, p. 2450096, 2024.

[11] S. S. Ghadikolaei, K. Hosseinzadeh, D. D. Ganji, and B. Jafari, "Hosseinzadeh, Ganji DD, Jafari B. Nonlinear thermal radiation effect on magneto Casson nanofluid flow with Joule heating effect over an inclined porous stretching sheet," Case Stud. Therm. Eng., vol. 12, pp. 176–187, 2018.

[12] D. Srinivasacharya and P. Jagadeeshwar, "Effect of Joule heating on the flow over an exponentially stretching sheet with convective thermal condition," Math. Sci., vol. 13, no. 3, pp. 201–211, 2019.

[13] M. N. Khan, S. Nadeem, N. Ullah, and A. Saleem, "Theoretical treatment of radiative Oldroyd-B nanofluid with microorganism pass an exponentially stretching sheet," Surf. Interfaces, vol. 21, p. 100686, 2020.

[14] A. M. Megahed, M. G. Reddy, and W. Abbas, "Modeling of MHD fluid flow over an unsteady stretching sheet with thermal radiation, variable fluid properties and heat flux," Math. Comput. Simul., vol. 185, pp. 583–593, 2021.

[15] E. Seid, E. Haile, and T. Walelign, "Multiple slip, Soret and Dufour effects in fluid flow near a vertical stretching sheet in the presence of magnetic nanoparticles," Int. J. Thermofluids, vol. 13, p. 100136, 2022.

[16] R. Biswas, S. Hossain, R. Islam, and S. Firoz, "Journal of Computational Mathematics and Data Science Computational treatment of MHD Maxwell nanofluid flow across a stretching sheet considering higher-order chemical reaction and thermal radiation," J. Comput. Math. Data Sci., vol. 4, p. 100048, 2022.

[17] M. A. Kumar and Y. D. Reddy, "Journal of the Indian Chemical Society Computational modelling of radiative Maxwell fluid flow over a stretching sheet containing nanoparticles with chemical reaction," J. Indian Chem. Soc., vol. 100, no. 1, p. 100877, 2023.

[18] M. Afrand, D. Toghraie, and B. Ruhani, "Effects of temperature and nanoparticles concentration on rheological behavior of Fe 3 O 4 -Ag / EG hybrid nanofluid : An experimental study," Exp. Therm. Fluid Sci., vol. 77, pp. 38–44, 2016.

[19] Z. Iqbal, E. Azhar, and E. N. Maraj, "Utilization of the computational technique to improve the thermophysical performance in the transportation of an electrically conducting Al 2 O 3 – Ag / H 2 O hybrid nanofluid," Eur. Phys. J. Plus, vol. 132, no. 544, p. 544, 2017.

[20] T. Hayat and S. Nadeem, "Results in Physics Heat transfer enhancement with Ag – CuO / water hybrid nanofluid," Results Phys., vol. 7, pp. 2317–2324, 2017.

[21] M. Usman, M. Hamid, T. Zubair, et al., "International Journal of Heat and Mass Transfer Cu-Al 2 O 3 / Water hybrid nanofluid through a permeable surface in the presence of nonlinear radiation and variable thermal conductivity via LSM," Int. J. Heat Mass Transf., vol. 126, pp. 1347–1356, 2018.

[22] I. Tlili, H. A. Nabwey, G. P. Ashwinkumar, and N. Sandeep, "3-D magnetohydrodynamic AA7072-AA7075/methanol hybrid nanofluid flow above an uneven thickness surface with slip effect," Sci. Rep., vol. 10, no. 1, p. 4265, Mar. 6 2020.

[23] W. Urmi, M. M. Rahman, and W. A. W. Hamazh, "An experimental investigation on the thermophysical properties of 40 % ethylene glycol based TiO 2 -Al 2 O 3 hybrid nanofluids," Int. Commun. Heat Mass Transf., vol. 116, p. 104663, 2020.

[24] P. S. P. Sudarsana and R. Ali, "Heat and mass transfer analysis of unsteady hybrid nanofluid flow over a stretching sheet with thermal radiation," SN Appl. Sci., vol. 2, no. 7, pp. 1–15, 2020.

[25] J. K. Madhukesh, K. R. Naveen, G. R. J. Punith, et al., "Numerical simulation of AA7072-AA7075 / water-based hybrid nanofluid flow over a curved stretching sheet with Newtonian heating : A non-Fourier heat flux model approach," J. Mol. Liq., vol. 335, p. 116103, 2021.

[26] S. Hazarika, S. Ahmed, and A. J. Chamkha, "Investigation of nanoparticles Cu, Ag and Fe3O4 on thermophoresis and vscous dissipation of MHD nanofluid over a stretching sheet in a porous Regime: A numerical modelling," Math. Comput. Simul., vol. 182, pp. 819–837, 2021.

[27] V. Puneeth, R. N. Anandika, S. Manjunatha, M. I. Khan, M. Imran Khan, A. Althobaiti, et al., "Muhammad. Implementation of modified Buongiorno's model for the investigation of chemically reacting rGo-Fe3O4-TiO2-H2O ternary nanofluid jet flow in the presence of bio-active mixers," Chem. Phys. Lett., vol. 786, p. 139194, 2022.

[28] K. Sarada, G. Fehmi, A. Amal, et al., "Case Studies in Thermal Engineering Impact of exponential form of internal heat generation on water-based ternary hybrid nanofluid flow by capitalizing non-Fourier heat flux model," Case Stud. Therm. Eng., vol. 38, p. 102332, 2022.

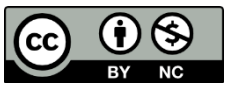
[29] S. Manjunatha, V. Puneeth, B. J. Gireesha, and A. J. Chamkha, "Theoretical Study of Convective Heat Transfer in Ternary Nanofluid Flowing past a Stretching Sheet," J. Appl. Comput. Mech., vol. 8, no. 4, pp. 1279–1286, 2022.

[30] N. Umar, S. Saleem, A. Al-Zubaidi, et al., "Thermal and mass species transportation in tri-hybridized Sisko martial with heat source over vertical heated cylinder," Int. Commun. Heat Mass Transf., vol. 134, p. 106003, 2022.

[31] S. A. Khan, T. Hayat, and A. Alsaedi, "Thermal conductivity performance for ternary hybrid nanomaterial subject to entropy generation," Energy Rep., vol. 8, pp. 9997–10005, 2022.

[32] F. Ali, A. Zaib, M. I. Khan, F. Alzahrani, and S. M. Eldin, "Irreversibility analysis in stagnation point flow of tri-hybrid nanofluid over a rotating disk; application of kinetic energy," J. Indian Chem. Soc., vol. 100, no. 2, pp. 2–5, 2023. 10.1016/j.jics.2022.100873

[33] D. G. Prakasha, M. V. V. N. L. Sudharani, K. G. Kumar, and A. J. Chamkha, "Comparative study of hybrid (graphene/magnesium oxide) and ternary hybrid (graphene/zirconium oxide/magnesium oxide) nanomaterials over a moving plate," Int. Commun. Heat Mass Transf., vol. 140, p. 106557, 2023.



All open access articles published in Transactions on Computational Modeling and Intelligent Systems (http://tcmis.org) are distributed under the terms of the CC BY-NC 4.0 license (Creative Commons Attribution Non-Commercial 4.0 International Public License as currently displayed at http://creativecommons.org/licenses/by-nc/4.0/legalcode) which permits unrestricted use, distribution, and reproduction in any medium, for non-commercial purposes, provided the original work is properly cited.